

Mesenchymal Differentiation Mediated by NF- κ B Promotes Radiation Resistance in Glioblastoma

Krishna P.L. Bhat,^{1,16,*} Veerakumar Balasubramaniyan,^{5,16} Brian Vaillant,^{7,16} Ravesanker Ezhilarasan,^{2,16} Karlijn Hummelink,¹ Faith Hollingsworth,¹ Khalida Wani,¹ Lindsey Heathcock,¹ Johanna D. James,¹ Lindsey D. Goodman,² Siobhan Conroy,⁶ Lihong Long,¹ Nina Lelic,⁸ Suzhen Wang,³ Joy Gumin,⁴ Divya Raj,⁵ Yoshinori Kodama,⁹ Aditya Raghunathan,¹⁰ Adriana Olar,¹ Kaushal Joshi,¹¹ Christopher E. Pelloski,¹² Amy Heimberger,⁴ Se Hoon Kim,¹³ Daniel P. Cahill,⁸ Ganesh Rao,⁴ Wilfred F.A. Den Dunnen,⁶ Hendrikus W.G.M. Boddeke,⁵ Heidi S. Phillips,¹⁴ Ichiro Nakano,¹¹ Frederick F. Lang,⁴ Howard Colman,^{15,17} Erik P. Sulman,^{2,17,*} and Kenneth Aldape^{1,17,*}

¹Department of Pathology

²Department of Radiation Oncology

³Department of Neuro-Oncology

⁴Department of Neurosurgery

The University of Texas, M.D. Anderson Cancer Center, Houston, TX 77030, USA

⁵Department of Neuroscience

⁶Department of Pathology and Medical Biology

University of Groningen, University Medical Center Groningen, Groningen 9713 AV, the Netherlands

⁷Department of Neurology, Seton Brain and Spine Institute, Austin, TX 78701, USA

⁸Department of Neurosurgery, Massachusetts General Hospital/Brain Tumor Center, Boston, MA 02114, USA

⁹Division of Pathology, Osaka National Hospital, National Hospital Organization, Chuo-ku, Osaka 540-0006, Japan

¹⁰Department of Pathology, Henry Ford Hospital, Detroit, MI 48202, USA

¹¹Department of Neurosurgery

¹²Department of Radiation Oncology

The Ohio State University, Columbus, OH 43210, USA

¹³Department of Pathology, Yonsei University College of Medicine, Seoul 120-752, Korea

¹⁴Department of Tumor Biology and Angiogenesis, Genentech, Inc., South San Francisco, CA 94080, USA

¹⁵Department of Neurosurgery, and Huntsman Cancer Institute, University of Utah, Salt Lake City, UT 84132, USA

¹⁶These authors contributed equally to this work

¹⁷These authors contributed equally to this work

*Correspondence: kbhat@mdanderson.org (K.P.L.B.), epsulman@mdanderson.org (E.P.S.), kaldape@mdanderson.org (K.A.)

<http://dx.doi.org/10.1016/j.ccr.2013.08.001>

SUMMARY

Despite extensive study, few therapeutic targets have been identified for glioblastoma (GBM). Here we show that patient-derived glioma sphere cultures (GSCs) that resemble either the proneural (PN) or mesenchymal (MES) transcriptomal subtypes differ significantly in their biological characteristics. Moreover, we found that a subset of the PN GSCs undergoes differentiation to a MES state in a TNF- α /NF- κ B-dependent manner with an associated enrichment of CD44 subpopulations and radioresistant phenotypes. We present data to suggest that the tumor microenvironment cell types such as macrophages/microglia may play an integral role in this process. We further show that the MES signature, CD44 expression, and NF- κ B activation correlate with poor radiation response and shorter survival in patients with GBM.

Significance

In this study, we characterize plasticity between the proneural (PN) and mesenchymal (MES) transcriptome signatures observed in glioblastoma (GBM). Specifically, we show that PN glioma sphere cultures (GSCs) can be induced to a MES state with an associated enrichment of CD44 expressing cells and a gain of radioresistance, in an NF- κ B-dependent fashion. Newly diagnosed GBM samples show a direct correlation among radiation response, higher MES metagene, CD44 expression, and NF- κ B activation, and we propose macrophages/microglia as a potential microenvironmental component that can regulate this transition. Our results reveal a mechanistic link between transcriptome plasticity, radiation resistance, and NF- κ B signaling. Inhibition of NF- κ B activation can directly affect radioresistance and presents an attractive therapeutic target for GBM.

INTRODUCTION

Glioblastoma (GBM) is the most common malignant primary central nervous system tumor in adults and remains resistant to current therapies (Furnari et al., 2007). Ample evidence exists to argue that GBM, as defined by histopathologic criteria, actually represents multiple distinct molecular entities (Huse et al., 2011). GBM can be segregated into subtypes based on gene expression signatures. Although the precise classifications have varied in the literature (Cooper et al., 2010; Huse et al., 2011; Phillips et al., 2006; Verhaak et al., 2010), two subtypes, termed proneural (PN) and mesenchymal (MES), appear robust and generally consistent among the classification schemes. GBMs in the MES subclass are predominantly primary tumors that arise de novo and, in some studies, exhibit a worse prognosis compared to PN tumors (Colman et al., 2010; Pelloski et al., 2005; Phillips et al., 2006), which may be related to the fact that a subset of the PN tumors displays mutations in the isocitrate dehydrogenase 1 gene (*IDH1*) as well as the glioma-CpG island methylator phenotype (G-CIMP), both favorable prognostic factors (Noussmeh et al., 2010; Verhaak et al., 2010). Conversely, MES tumors are G-CIMP⁻, exhibit wild-type (WT) *IDH1*, and contain alterations in *NF1* (Noussmeh et al., 2010; Verhaak et al., 2010).

Although a wealth of data on molecular alterations in GBM continues to accumulate, the availability of relevant models that mirror these alterations is limited. Current evidence points toward the existence of a small fraction of tumor-initiating cells in the bulk tumor that also exhibit radioresistant properties (reviewed in Chen et al., 2012). However, the genetic and epigenetic alterations underlying TICs derived from glioma sphere cultures (GSCs) are less characterized. Whereas initial studies identified CD133 as a tumor-initiating marker, CD133⁻ subpopulations that resemble the MES subtype also retain the capacity to form tumors in orthotopic transplantation models (reviewed in Stopschinski et al., 2012). Consequently, additional cell surface antigens have been proposed as tumor-initiating markers for GSCs including CD44 (Brescia et al., 2012; Jijiwa et al., 2011), a marker that is enriched in cancer stem cells as well as those that undergo epithelial to MES transition (EMT; Zöller, 2011). Interestingly, MES transition has also been shown to occur in GBM and can be induced by master transcription factors (TFs), STAT3, C/EBP β , and TAZ (Bhat et al., 2011; Carro et al., 2010). Whether this transition occurs in a cell-intrinsic manner or can be influenced by factors secreted in the tumor microenvironment is not known. Furthermore, whether MES differentiation leads to enrichment of the CD44 subpopulation in a fashion similar to other solid tumors remains unexplored. Finally, PN tumors have been found to give rise to MES recurrences, suggestive of a PN to MES transition (Phillips et al., 2006). Therefore, understanding the mechanistic basis of MES differentiation may have implications for the treatment of GBM.

RESULTS

Patient-Derived GSCs Bear Resemblance to PN and MES Signatures

In the context of molecular subtypes reported for GBM, we examined whether GSCs isolated from patient-derived tumors show similar characteristics. Forty-one GBM tumors were sub-

jected to culture conditions according to published protocols and successful expansion as neurospheres was observed in 33 cases (Table S1 available online). Seventeen GSCs that were expanded earliest were chosen for microarray analysis to identify molecular subtypes using unsupervised algorithms. Using 500 probe sets with the highest variability in gene expression, two clusters of coexpressed genes were readily apparent by hierarchical clustering (Figure 1A). These two clusters for the most part were well defined, although some GSCs did not readily fit in this pattern (e.g., GSC6-27, 30, and 46). The primary or recurrent status of the parental tumor of origin had no bearing on the cluster segregation (cluster 1 = 33% versus cluster 2 = 36% recurrent tumors; Figure 1A). To understand the functional significance of these two gene clusters, we performed Gene Ontology (GO) analysis using the Database for Annotation, Visualization and Integrated Discovery (DAVID) webtool (Dennis et al., 2003). Cluster 1 GO terms were enriched for wound response, vasculature formation, and cell motility gene signatures (Figure 1B), whereas cluster 2 showed predominant association with differentiated neural or glial cell functions and homeostatic activities (Figure 1B). Importantly, cluster 1 showed significant similarity only to the MES GBM subclass by Gene Set Enrichment Analysis (GSEA; Subramanian et al., 2005; Figure 1C), with 89 out of the top 500 enriched genes being MES (Figure S1A; Table S2). Similarly, cluster 2 predominantly comprised PN genes (98/500; Figures 1C and S1A; Table S2). Supervised clustering using the TCGA classification (Verhaak et al., 2010) showed a similar grouping of the GSCs at the first branch of the dendrogram compared to the unsupervised clustering (Figure S1B). GSC6-27 and 30 displayed characteristics of both MES and PN gene signatures. GSC11 and 30 were also enriched for Classical (CL) signatures. EGFR amplification, usually restricted to the CL subtype, was seen in 5 out of the 14 GSCs and appeared distributed between the PN and MES subtypes (3 PN and 2 MES; Figure S1C). *NF1* homozygous inactivating mutations were observed in GSC6-27 (exon 39) and GSC28 (exon 50 and exon 38; Figure S1D), both GSCs that had MES characteristics consistent with the TCGA analyses (Verhaak et al., 2010). Quantitative RT-PCR (qRT-PCR) and immunoblotting of basal expression of key PN/MES markers (Table S3) were concordant with microarray results (Figures S1E and S1F).

To rule out the possibility of nonneoplastic cells being enriched in the GSC isolation procedure, we tested for loss of heterozygosity (LOH) on chromosome 10q, a frequently deleted region in adult GBM (Pietsch and Wiestler, 1997), and found LOH in 12 out of the 13 GSCs, confirming their neoplastic origin (Figure S1G). Implantation of 5×10^5 or fewer unsorted GSCs caused formation of high-grade gliomas (HGGs) in a majority of the cases (13/17) with predominant histologic features of this disease (Tables S4 and S5; Figure S1H). A subset of the tumors exhibited microvascular proliferation and/or pseudopalisading necrosis, both hallmarks of GBM (Figure S1H). Thus, despite differential gene expression signatures, GSCs formed tumors that were histologically similar.

GSCs Differ in the Transcriptome and Epigenetic Profiles When Compared to the Originating Tumor

Next, we examined whether gene expression patterns observed in the GSCs and xenografts matched with the respective

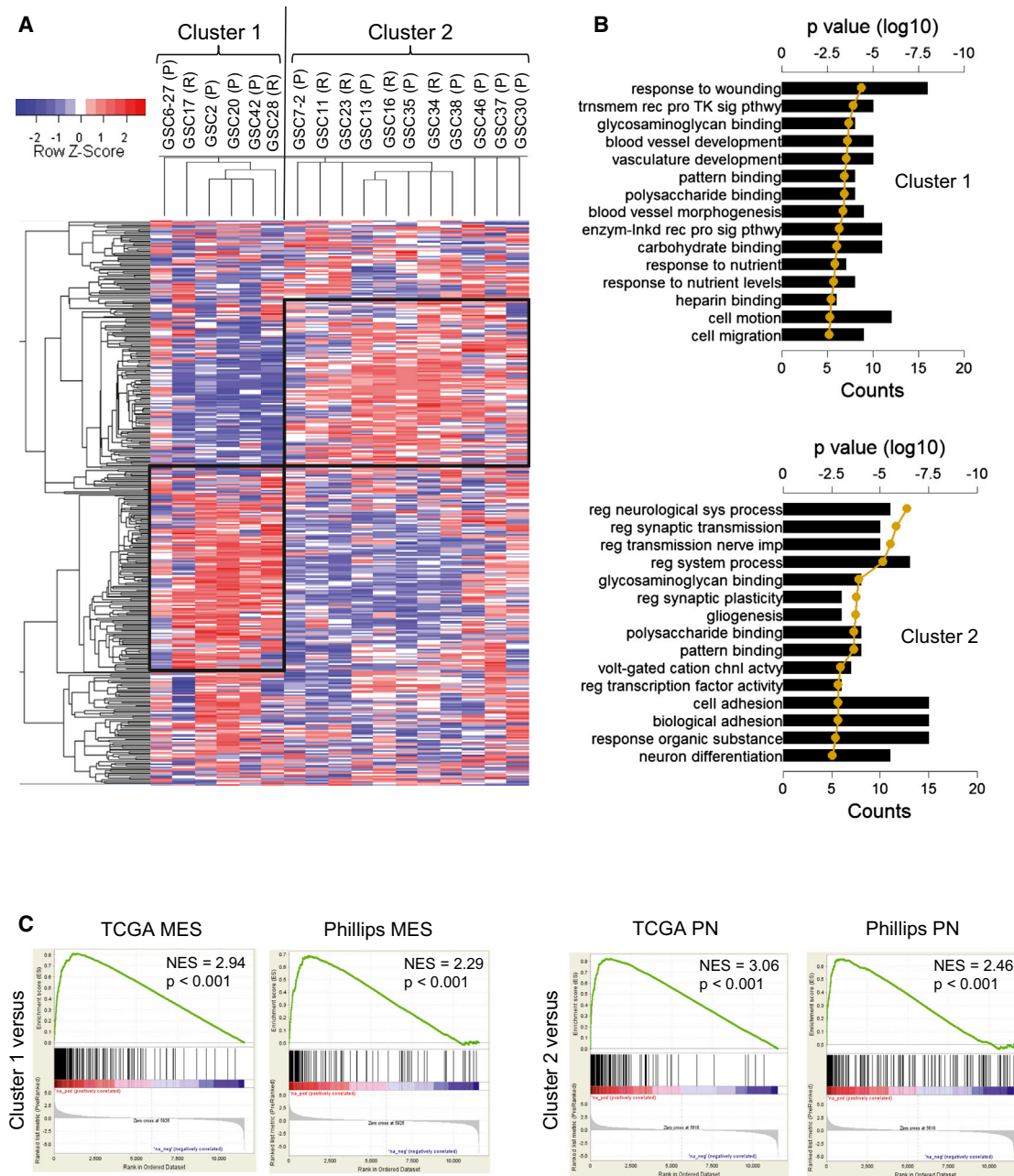


Figure 1. Patient-Derived GSCs Bear Resemblance to PN and MES Signatures

(A) Unsupervised hierarchical analysis of the top 500 highest median absolute deviation genes from expression microarray of 17 GSCs is shown. Expression data was Z score corrected for display; relatively lower expression is shown in blue and higher expression is shown in red (see color key). Two large clusters, cluster 1 (128 genes) and cluster 2 (102 genes), were identified (shown as black boxes). The vertical black line identifies the first dendrogram splitting of the GSCs. Primary (P) or recurrent (R) status of the GSCs is indicated.

(B) The top 20 gene ontology (GO) terms associated with cluster 1 (left) and cluster 2 (right) from the unsupervised GSC hierarchical cluster analysis are shown. GO terms are ranked by p value. The black bars show the number of genes that is common between the GO term's gene set and the respective cluster gene set. The golden line is the log₁₀ of the p value as determined by DAVID functional analysis.

(C) GSEA enrichment plots of GSC cluster 1 high (top row) and cluster 2 high (bottom row) gene lists versus queried gene lists are shown (see [Supplemental Experimental Procedures](#) for data source). The normalized enrichment scores (NES) and the p values are shown for each plot. See also [Figure S1](#) and [Tables S1, S2, and S3–S5](#).

parental GBMs from which they were derived. To determine the association of a sample with either a PN or MES gene expression signature, we calculated a metagene score for each sample

using a set of four PN (*DLL3*, *OLIG2*, *ASCL1*, and *NCAM1*) and four MES (*YKL40*, *SERPINE1*, *TIMP1*, and *TGFBI*) genes, seven out of the eight of which were subset defining in published data

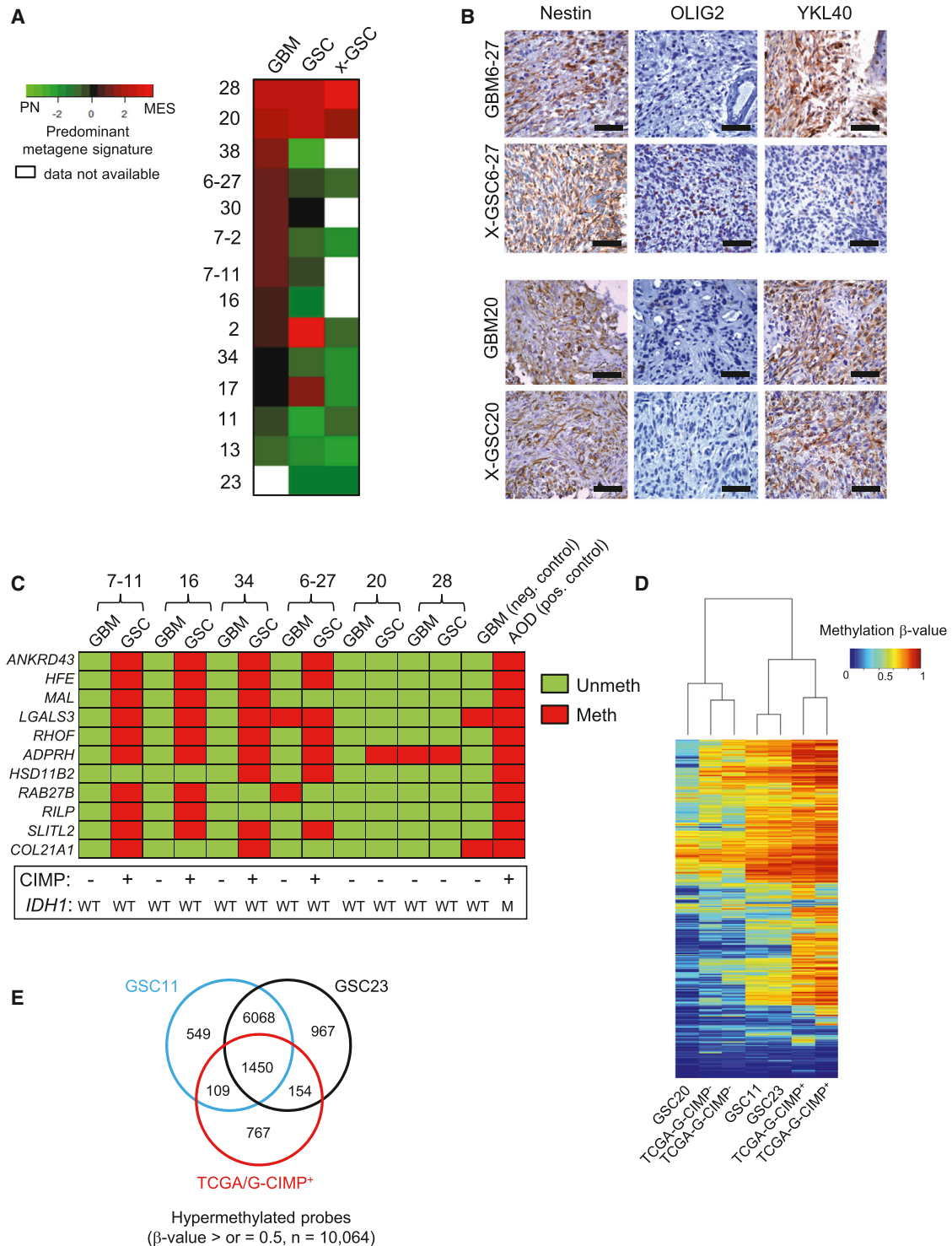


Figure 2. GSCs Differ in the Transcriptome and Epigenetic Profiles when Compared to the Originating Tumor

(A) Heatmap of the predominant signature of initiating GBM, derived GSC, and xenograft for 14 samples is shown. A PN and MES qRT-PCR-based metagene was calculated for each sample and then compared to each other after Z score correction. Green shades represent a predominantly PN signature, red a MES one, and black a relatively balanced expression of both, as indicated in the figure.

(B) IHC analysis of Nestin, OLIG2, and YKL40 expression in patient-matched GBM and xenografts of GSCs is shown. Scale bar: 50 μm.

(C) Methylight profiling of GBMs and their derivative GSCs for G-CIMP status is shown. Eleven markers were tested for presence of methylation on their promoters and coded as red if methylated and green if unmethylated. Samples were deduced as G-CIMP if >50% of the loci showed methylation. A GBM and

(legend continued on next page)

sets (Phillips et al., 2006; Verhaak et al., 2010). Using this approach, each sample could be ranked according to its metagene score as being predominantly PN or MES. Surprisingly, we found that most GSCs that arose from MES tumors lost MES characteristics and exhibited a higher PN metagene (Figure 2A). GSC20 and GSC28, both of which originated from highly MES tumors with histological hallmarks of gliosarcoma (Figure S2A), maintained their MES state in culture and as xenografts. With the exception of GSC2 and GSC17 (which lost MES features gained in culture), all PN GSCs maintained their PN status when examined in xenografts. Alterations in growth factor supplements to culture media did not influence gene expression signatures in established GSCs, although neurosphere formation was dependent on EGF (Figures S2B and S2C). Immunohistochemical (IHC) analysis on xenografts showed absence of the MES marker YKL40 in GSCs derived from MES tumors, which instead acquired the PN marker OLIG2 (Figures 2B and S2D). This contrast was not observed in the MES GSC20 that retained YKL40 expression in the xenograft, similar to the parental tumor, but lacked OLIG2 expression in both (Figure 2B). These findings imply that the GSC isolation protocol generally favors a loss of MES and gain of PN features from patient to xenograft.

Given the tight association of the G-CIMP signature with the PN subtype (Noushmehr et al., 2010), we asked whether PN GSCs are G-CIMP⁺. To test this, we used a previously reported G-CIMP signature panel that shows correlation with array-based methylation platforms (Noushmehr et al., 2010). Eleven hypermethylated gene regions were chosen based on feasibility and reproducibility in archival tumor-derived DNA and deemed G-CIMP⁺ based on percentage loci that were hypermethylated (>50%). Consistent with a drift toward a PN signature from tumor to GSC, we observed that PN GSCs were G-CIMP⁺ compared to their parental tumors that were G-CIMP⁻ (Figures 2C and S2E). To the contrary, MES GSCs 20 and 28 remained G-CIMP⁻ similar to their parental tumors (Figure 2C). To test for the extent of similarity to the previously described G-CIMP signature on a genome-wide scale, we profiled three GSCs using the Illumina Infinium methylation array (Figure 2D). Upon cross-examination with TCGA tumors, PN GSCs 11 and 23 segregated with G-CIMP⁺ tumors, while GSC20 clustered with the G-CIMP⁻ cases. Overall, GSCs 11 and 23 showed greater hypermethylation compared to GSC20 (Figure S2F) and showed an ~70% enrichment of G-CIMP signature genes, although numerous distinct non-G-CIMP loci also appeared hypermethylated in these GSCs (Figure 2E). Taken together, our data suggest that PN GSCs can exhibit hypermethylation patterns (henceforth named CIMP) with similarities to G-CIMP even in the absence of *IDH1* mutations.

Molecular Signatures Differ between GBM and Their Derivative GSCs Even in Early Passages

Based on our initial findings, two possibilities were considered: (1) culturing of freshly resected GBMs in serum-free media sup-

plemented with growth factors preferentially induces a PN/CIMP⁺ signature in culture, or (2) most undifferentiated GSCs are innately PN/CIMP⁺, but the microenvironment in human tumors induces a reversible MES/CIMP⁻ differentiation, which is not entirely recapitulated in vitro or in xenografts of immunocompromised mice. To discern which one of these can be attributed to a general MES/CIMP⁻ to PN/CIMP⁺ drift, and to reduce the potential of artifacts from long-term culture, we examined freshly resected tissues and their derivative serial passage GSCs for gene expression and methylation signatures as soon as sufficient starting material was available for analyses. Strikingly, even in early passages (fewer than five), we observed that GSCs showed PN characteristics despite having a MES origin (Figure S2G). Moreover, these early passage GSCs were CIMP⁺ in contrast to their parental tumors, which were CIMP⁻ (Figure S2H). These observations, taken together with previous studies showing requirement of extended passages for the induction of the G-CIMP phenotype by *IDH1* mutation (Lu et al., 2012; Turcan et al., 2012), favor a model in which a majority of undifferentiated GSCs already exist in a PN/CIMP⁺ state and are selectively enriched under proliferating conditions.

CD44 Is Enriched in the MES Subtype and Is Inversely Correlated with OLIG2 Expression

Next, to test whether the differential molecular signatures have a bearing on their biological properties, we expanded our repertoire of GSCs. We first examined the expression of cell surface markers that have been used to define tumor-initiating potential. We observed enrichment of CD15 specifically in the PN/CIMP⁺ subclass of GSCs (e.g., GSC11, GSC23, and GSC34) that also expressed equal or smaller percentages of CD44 (Figure 3A), although the ratio of CD15 to CD44 varied with passage or confluence of spheres. MES/CIMP⁻ GSCs (e.g., GSC20, GSC28, and GSC2) did not express appreciable levels of CD15 but predominantly expressed CD44 (Figure 3A). Comparison of CD15 and CD44 expression among GSCs with a range of passage times showed no correlation (Figures S3A and S3B). Using OLIG2 as a surrogate for CD15 (Figure S3C) as previously shown (Son et al., 2009), we found a mutually exclusive pattern of inter- and intratumoral staining with CD44 (Figures 3B, 3C, and S3D), implying that these were indeed distinct tumor populations. Furthermore, PN tumors expressed higher levels of *OLIG2* whereas MES tumors predominantly expressed *CD44* and the expression of *OLIG2* and *CD44* was inversely correlated (Figures 3D and S3E). Additionally, CD44^{high} subpopulations within PN/CIMP⁺ GSCs showed enrichment of MES markers (Figure S3F). Thus, whereas unsorted GSCs formed tumors upon transplantation irrespective of exclusive expression of tumor initiation markers, CD15 (e.g., GSC7-11) or CD44 (e.g., GSC20), the proportion of the cell surface expression of CD44 appeared to correlate with a MES state.

an anaplastic oligodendroglioma (AOD) sample were used as negative and positive controls, respectively. The *IDH1* and G-CIMP status of all samples is shown below.

(D) Heatmap shows the unsupervised clustering of 1,138 differentially hypermethylated probes from the G-CIMP signature.

(E) Venn diagram shows the number of hypermethylated probes (β values ≥ 0.5) in GSCs 11, 23, and TCGA G-CIMP⁺ tumors.

See also Figure S2.

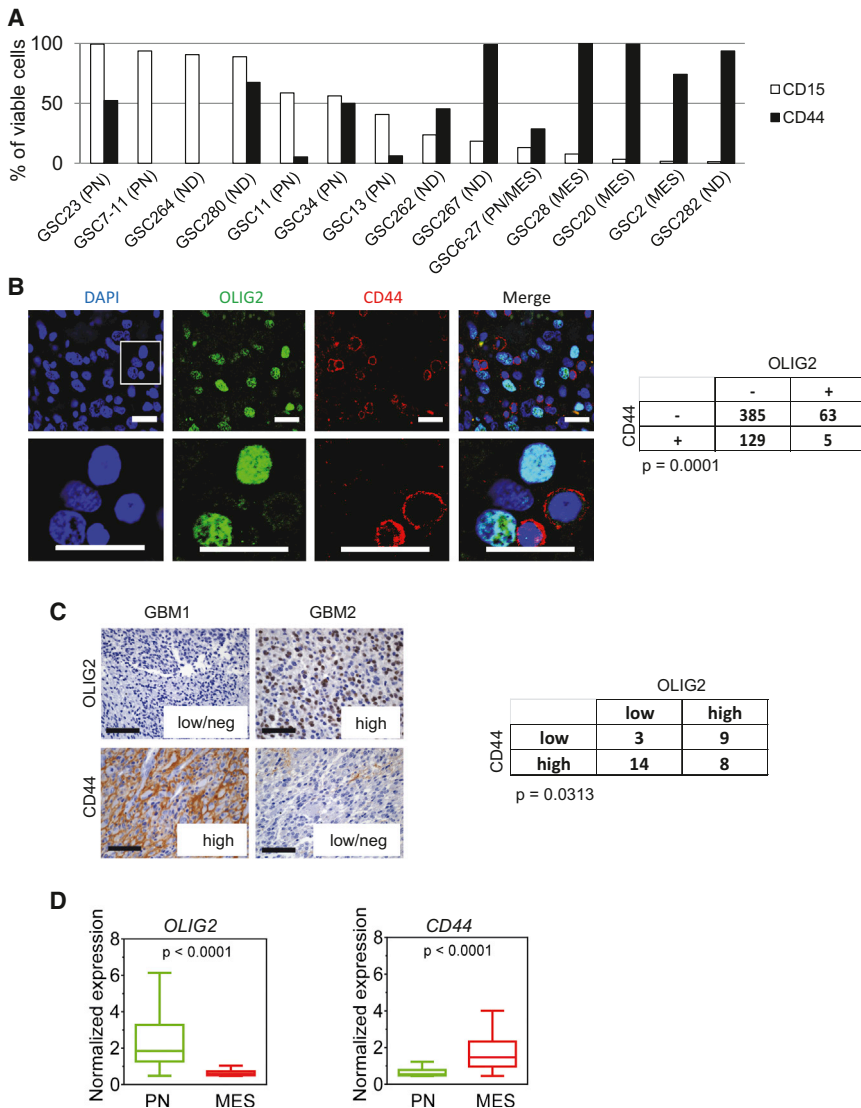


Figure 3. CD44 Is Enriched in the MES Subtype and Is Inversely Correlated with OLIG2 Expression

(A) CD15 and CD44 of various GSCs were determined by flow cytometry. Bar graph indicates percentage of viable cells that express these markers at the earliest passage tested. ND, not determined.

(B) Immunofluorescent staining of OLIG2 (green) and CD44 (red) in human GBM tumors shows a mutually exclusive pattern of staining. Scale bar: 20 μ m. The merged image of CD44/OLIG2 is shown on the right against 4',6-diamidino-2-phenylindole (DAPI)-stained nuclei (blue). Enlarged inset is shown in the lower panel (scale bar: 20 μ m). Quantification of staining in three random fields of three independent tumors and the p value from chi-square test are shown on the right.

(C) Representative IHC images of OLIG2 and CD44 expression in human GBM samples are shown. Scale bar: 50 μ m. The table to the right shows the number of tumors expressing OLIG2/CD44. Tumors were classified as low/negative, intermediate, or high depending on the extent of expression in the overall tumors. p value was calculated using chi-square test.

(D) Box plots show the normalized median expression of *OLIG2* and *CD44* in TCGA tumors based on Phillips and TCGA classification. Boxes show median 25th and 75th percentiles, while whiskers show the 5th and the 95th percentiles. The p value was determined using a nonparametric Wilcoxon test.

See also Figure S3.

PN/CIMP⁺ and MES/CIMP⁻ GSCs Display Differential Sensitivity to Radiation

To test whether GSCs with varied transcriptome, methylation, and cell surface antigen expression patterns also exhibit differential treatment responses, we examined the consequence of clinically relevant fractionated ionizing radiation (IR; 2.5 Gy \times 4) on mice 2–3 weeks after orthotopic implantation of GSCs. PN/CIMP⁺ GSCs (7–11 and 23) showed significantly improved median survival (5–9 weeks) upon IR treatment, whereas GSC20 showed no statistical difference and GSC267 showed modest survival (~2 weeks) improvement compared to untreated controls (Figure 4A). Because glioma cells predominantly arrest in the G2/M phase of cell cycle in response to IR (Mir et al., 2010), we asked whether the two subtypes of GSCs showed fundamental differences in this mode of arrest. Indeed, PN/CIMP⁺ GSCs showed dramatic accumulation of cells in G2/M, whereas MES/CIMP⁻ GSCs showed only a modest arrest (Figure 4B). In addition, although both subtypes of GSCs showed comparable γ -H2AX foci formation at early time points, MES/

CIMP⁻ GSCs (2, 20, and 267) showed enhanced repair ability as evidenced by the reduced number of foci at 24 hr compared to PN/CIMP⁺ GSCs (Figure 4C), consistent with the lack of G2/M arrest. Consequently, the PN/CIMP⁺ GSCs underwent profound apoptosis (Figure 4D) with reduced neurosphere formation compared to MES/CIMP⁻ GSCs (Figure 4E). We further observed a similar radioresistant CD44^{high} population within the PN/CIMP⁺ GSCs (Figures S4A–S4C).

TNF- α Mediates MES Differentiation in an NF- κ B-Dependent Fashion

Despite originating from MES tumors, the lack of MES signature in xenografts led us to hypothesize that specific factors in the human tumor microenvironment could alter the transcriptome and epigenetic signatures of GSCs, but these features are not entirely recapitulated in immunocompromised mice. In search of such signaling molecules, we noted that the TCGA analyses showed specific enrichment of genes in the TNF- α receptor superfamily and the NF- κ B pathway in the MES subclass of tumors that also expressed high levels of *YKL40* and *CD44* (Riddick and Fine, 2011; Verhaak et al., 2010). Additionally, prior studies have shown the association of a hypoxic signature and the NF- κ B pathway to HGGs (Murat et al., 2009). We

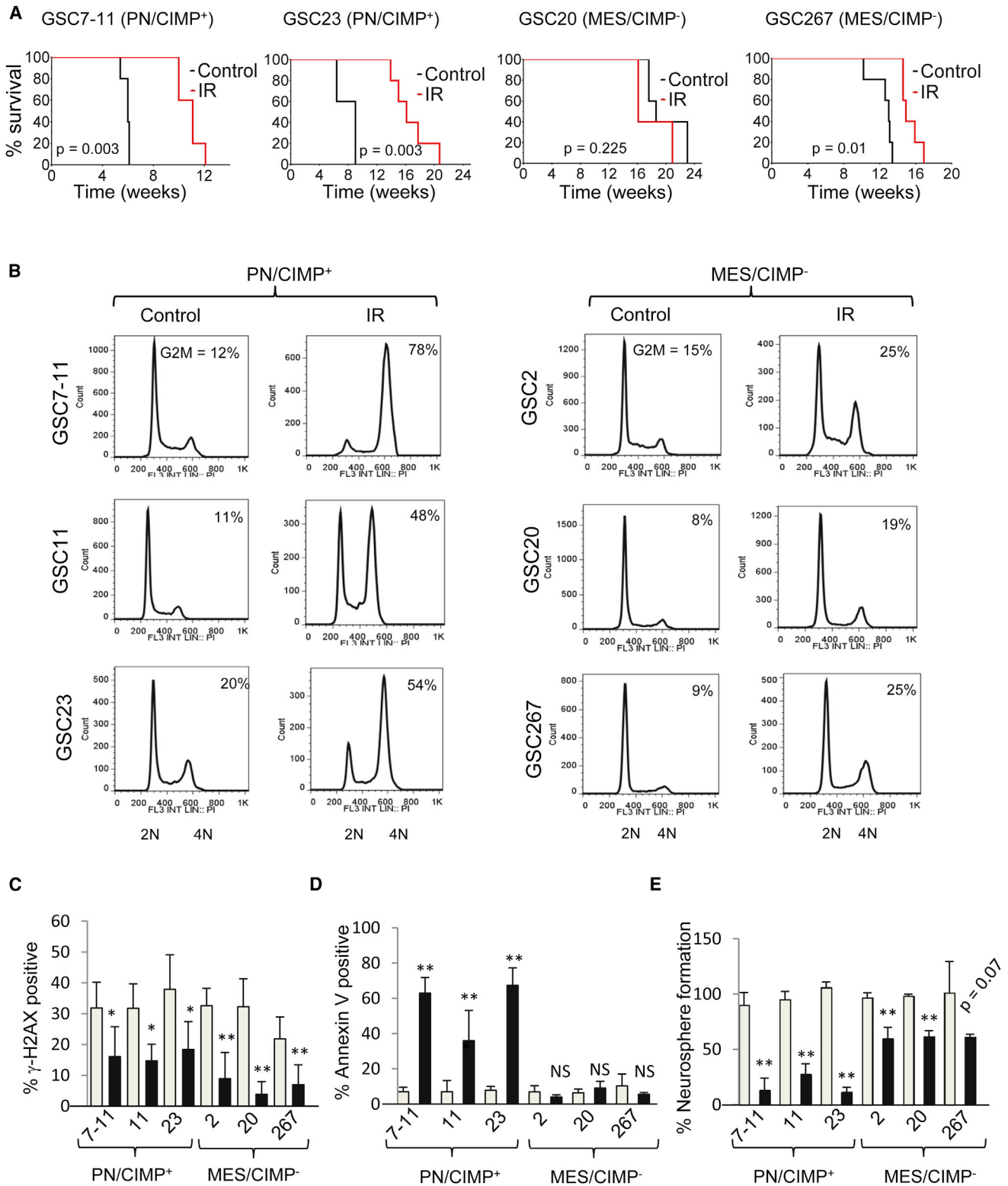


Figure 4. PN/CIMP⁺ and MES/CIMP⁻ GSCs Display Differential Sensitivity to Radiation

(A) Kaplan Meier curves show the survival of mice implanted with PN/CIMP⁺ (7-11 and 23) or MES/CIMP⁻ (20 and 267) GSCs at 5×10^5 cells per mouse with or without fractionated intracranial radiation (2.5 Gy \times 4). t test was used to assess statistical significance.

(B) Cell cycle analysis of GSCs treated with 6 Gy IR is shown. The percentage of cells in the G2M phase is indicated within each cell cycle plot.

(legend continued on next page)

hypothesized that cytokines that can trigger NF- κ B or alternative TF signaling pathways could result in MES differentiation and influence the proportion of CD44^{high} subpopulations. To test this, we treated PN/CIMP⁺ GSCs 11, 23, and 34 with similar concentrations of interleukin (IL)-6, IL-8, IL-10, TGF- β , or TNF- α , all of which are constituents of the GBM microenvironment (Charles et al., 2011). TNF- α treatment resulted in a dramatic gain of CD44 expression, an effect not seen with any of the other cytokines tested (GSC34, Figure 5A; GSC11 and 23, data not shown), and this effect was blunted by transduction with a nondegradable mutant form of I κ B (I κ B superrepressor [I κ B-SR]), indicating an NF- κ B-dependent effect (Figure 5B). Interestingly, the CIMP positivity of the GSCs remained unaltered in response to TNF- α treatment (Figure 5C), implying that the regulation of CIMP can be uncoupled from NF- κ B-mediated MES differentiation in GSCs. However, long-term effects of TNF- α and/or other potential modifiers of CIMP status are worthy of further exploration.

To further characterize the extent of MES differentiation, we performed microarray analysis of GSCs treated with TNF- α and found significant enrichment of genes involved in wound healing and vasculature development, as well as the NF- κ B cascade and regulation of cell-death-related genes (Figure 5D), suggesting that in addition to the canonical NF- κ B pathway, TNF- α induces a parallel MES differentiation in GSCs, which was further confirmed by qRT-PCR (Figure S5A). Moreover, genes induced by TNF- α were significantly similar to the GBM MES subclass (Figure S5B). Interestingly, although a global reduction of the PN signature was not observed, a significant downregulation of *OLIG2*, *PDGFRA*, and *DLL3* transcripts were seen with TNF- α treatment (data not shown). Physiological concentrations (100 pg/ml) of TNF- α were sufficient to cause induction of YKL40 and CD44 (Figures S5C and S5D), which was temporally preceded by activation of NF- κ B, as judged by serine 536 (ser 536) phosphorylation (Figure S5D). Furthermore, we identified macrophages/microglia as the stromal cell type that can potentially induce MES differentiation (Figures S5E–S5I) and that MES/CIMP⁻ GSCs show selective susceptibility to minocycline, an inhibitor of microglial activation and NF- κ B signaling (Figures S5J–S5N; Dagainakatte and Gutmann, 2007; Markovic et al., 2011).

Pretreatment of PN/CIMP⁺ GSCs with TNF- α strongly reduced the G2/M accumulation in response to IR (Figure 5E) as well as the number of γ -H2AX foci (Figure S5O), and these effects were inhibited by pretreatment with I κ B-SR, indicating that TNF- α promotes MES differentiation coupled with increased radioresistance in an NF- κ B-dependent manner. We noted that although long-term treatment of GSCs with TNF- α (5 ng/ml) reduced the neurosphere formation (Figure S5P), exposure of GSCs to IR caused significantly higher neurosphere efficiency

in the presence of TNF- α compared to untreated controls, suggesting a radioprotective effect of TNF- α (Figure S5P). To examine this in vivo, we expressed firefly luciferase in GSC23 to monitor tumor kinetics using bioluminescent imaging. As expected, IR caused a strong decrease in tumor volume (Figure 5F), and a similar growth inhibition was seen with TNF- α treatment alone, consistent with our in vitro observations. However, a combination of TNF- α and IR caused significant expansion of the tumor, and the cells appeared similar in volume to the control group. Overall, our findings indicate that the induction of MES differentiation and enrichment of CD44 by NF- κ B activation promotes radioresistance in PN/CIMP⁺ GSCs.

NF- κ B Controls Master TFs of MES Differentiation in GSCs

Next, we explored how NF- κ B pathway activation integrates into the MES signaling network and its relation to master TFs (STAT3, C/EBP β , and TAZ) known to induce this signature. We found that both total and phosphorylated forms of p65 (ser 536) were significantly higher in MES/CIMP-GSCs 2 and 20 when compared to PN/CIMP⁺ GSCs 11 and 23 (Figure 6A). The expression of STAT3 and C/EBP β as well as phosphorylation at tyrosine 705 of STAT3 (which promotes nuclear translocation and DNA binding of STAT3) were also higher in the MES/CIMP⁻ GSCs (Figure 6A). Similar increases in MES proteins and master TFs were seen in the CD44^{high} subpopulation when compared to those that were CD44^{low} (Figures 6B and 6C). CD44 expression also positively correlated with *STAT3*, *CEBPB*, and *TAZ* expression as well as NF- κ B pathway activation in human GBMs (Figure 6D). Although these TFs showed strong association with the MES signature, classic EMT inducers *SNAIL*, *SLUG*, and *TWIST1* were not robustly associated (Figure S6A).

To test whether NF- κ B mediates MES reprogramming via master TFs, we treated GSC11 with TNF- α at various time points and analyzed the temporal expression of these proteins by western blotting. TNF- α -induced phosphorylation of p65 preceded the induction of YKL40, STAT3, C/EBP β , and TAZ, an effect that was negated by pretreatment with I κ B-SR, indicating that the master TFs act downstream of the NF- κ B pathway (Figures 6E and 6B). Furthermore, upregulation of *STAT3*, *CEBPB*, and *TAZ* mRNA was significantly inhibited by I κ B-SR pretreatment (Figures 6F and 6B). Finally, concomitant silencing of *STAT3*, *C/EBP β* , and *TAZ* caused strong reduction of *CD44* and *YKL40* induced by TNF- α (Figures 6G and 6B). Taken together, these data indicate that NF- κ B promotes MES differentiation in GSCs via induction of master TFs. Interestingly, GSC13, which originated from a PN tumor (Figure 1C), did not exhibit MES differentiation even upon long-term culture in TNF- α , suggesting that some PN GSCs are resistant to NF- κ B-mediated MES differentiation (Figure S2C).

(C) γ -H2AX foci formation assay is shown. Gray bars indicate number of foci after 6 hr irradiation whereas black bars show foci after 24 hr. At least 25 nuclei were counted. Error bar indicates \pm SEM. t test was used to assess statistical significant differences. * $p < 0.05$, ** $p < 0.005$.

(D) Percentage of cells that were positive for annexin V staining 96 hr post irradiation is shown as bar graphs. Gray bars indicate percentage of cells in untreated population whereas black bars show percentage of annexin-V-positive cells exposed to 6 Gy IR. Error bar indicates \pm SD. t test was used for statistical significance. ** $p < 0.005$; NS, not significant.

(E) Neurosphere formation efficiency was determined by setting the number of spheres formed in control groups at 100% (gray bars) and compared to those exposed to 3 Gy IR (black bars). Error bar indicates \pm SD. t test was used for statistical significance. ** $p < 0.005$.

See also Figure S4.

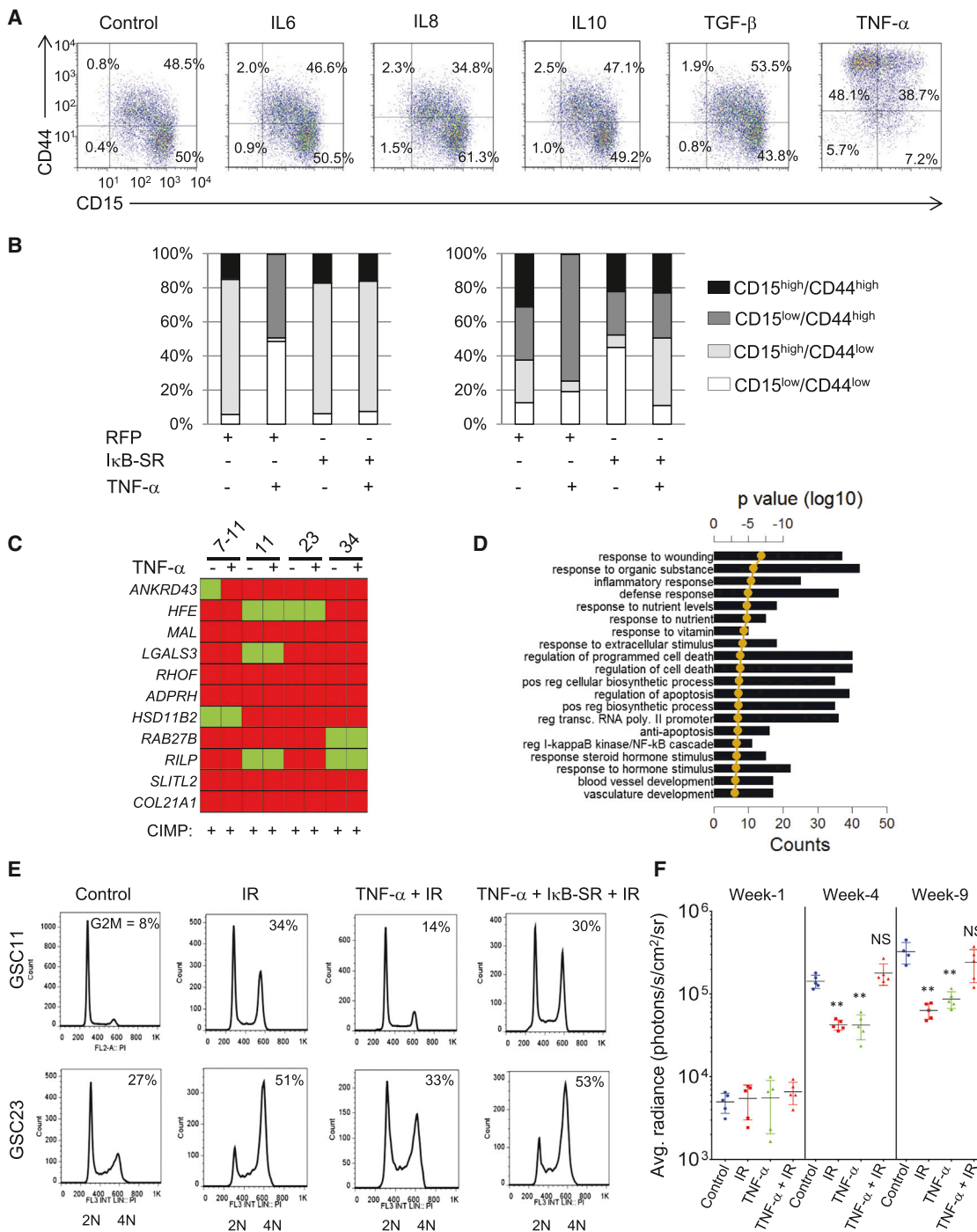


Figure 5. TNF-α Mediates MES Differentiation and Radioresistance in an NF-κB-Dependent Fashion

(A) FACS analysis of expression of CD15 and CD44 in GSC34 after 96 hr treatment with 10 ng/ml of indicated cytokines is shown. Percentage of cells in each quadrant is shown.

(B) Expression of CD15 and CD44 after TNF-α (96 hr, 10 ng/ml) with or without pretreatment with IκB-SR adenovirus or control RFP adenovirus 24 hr prior to TNF-α treatment by flow cytometry is shown. The stacked bar shows the percentage of CD15/CD44-expressing cells after various treatments.

(C) Methylight profiling of GSCs after 2 weeks of TNF-α treatment is shown.

(D) The top 20 GO terms associated with 1.5-fold or greater TNF-α-induced genes in GSC11 are ranked by lowest p value. Bar graphs show the number of genes overlapping between the GO category and the query gene list. The golden line is the DAVID functional analysis determined log₁₀ of p values.

(E) Cell cycle analysis of GSCs after treatments is indicated. The percentage of cells in the G2/M phase is indicated within each cell cycle plot.

(F) Tumor volume measurement of GSC23-pCignal lenti-CMV-luc cells injected intracranially into Foxn1^{nu} mice is shown. Mice were imaged 2–3 weeks after implantation as the first time point (denoted as week 1), after which the radiation group received four cycles of 2.5 Gy IR on consecutive days. Mice were subject to

(legend continued on next page)

MES Differentiation, CD44 Levels, and NF- κ B Activation Are Predictive of Radiation Response in GBM

Because activation of NF- κ B caused both MES differentiation and enrichment of CD44 populations in GSCs, we performed in-depth analyses of NF- κ B activation in GBM. Among previously annotated direct targets of NF- κ B, MES GSCs as well as tumors (Table S6) showed a 36% enrichment (induced to a 1.5-fold or greater expression) of these targets when compared to PN counterparts, which showed only a 6% enrichment (Figure S7A). Seventeen NF- κ B target genes appeared commonly induced in both MES GSCs and GBMs, which included *CD44*, proinflammatory cytokines *IL1B* and *IL8*, chemokines *CCL2* and *CXCL5*, prostaglandin enzyme cyclooxygenase 2 (*COX2*), and the downstream target of TNF- α stimulation *TNFAIP3* that has been previously shown to be associated with GBM (Hjelmeland et al., 2010; Murat et al., 2009). Thus, the MES phenotype in GSCs and GBM was accompanied by activated NF- κ B signaling, and CD44 is an integral component of this signature.

We next examined the association of these variables with radiation response and treatment outcome in a cohort of newly diagnosed GBM patients (Table S7). We used a previously defined radiation response scoring criteria (Pelloski et al., 2005) by comparing the maximal area of enhancement between the pre- (i.e., within 1 month of the start of radiation) and the post-RT magnetic resonance imaging (MRI; Figure 7A). Examination of the PN/MES status showed correlation between MES composite metagene (see Supplemental Experimental Procedures for details) and progression following RT (nonresponders) whereas a PN composite metagene correlated to patients with stable or reduced disease following RT, even in patients with WT *IDH1* tumors (Figures 7B and 7C). After adjusting for patient age (≤ 50 years versus >50 years), *IDH1* status (mutant versus WT), and Karnofsky Performance Status (KPS; ≤ 70 versus >70), only the MES metagene remained a significant predictor of RT response (Table S8). Patients with a higher MES metagene (upper two-thirds of the metagene quartile) also showed reduced survival irrespective of *IDH1* status (Figures 7D and 7E). Next, we evaluated whether CD44 and OLIG2 expression could be used as serviceable markers for MES and PN states, respectively. Patients with higher expression of CD44 showed a striking association with poor response to radiation and lower survival compared to those with lower CD44, and conversely, patients with high OLIG2 were more likely to be responders to radiation and better survivors (Figures 7F–7I; Figures S7B–S7E). Additionally, using an antibody specific for phosphorylated p65 (ser 276), a transcriptionally active form of NF- κ B, as well as its target *COX2* (Figure S7F), we found significant association of the expression of these proteins to nonresponders compared to those with a favorable response to radiation (Figures 7J and 7K; Figures S7G and S7H). Whereas intermediate and high *COX2* expression were associated with poor survival (Figures 7L and S7I), p-p65 expression showed a similar trend but did not reach statistical significance (data not shown).

Finally, to characterize intratumoral PN to MES transition in human GBMs, we closely examined the temporal distribution of multiple markers by IHC on serial paraffin-embedded sections (Table S9). The expression of these markers ranged from pockets of negative expression to those with strong positivity. Importantly, OLIG2^{low} and CD44^{high} areas (MES signature) coincided with p-p65 positivity (Figure 8A; Table S9). The extent of macrophages/microglia infiltration (as judged by IBA staining) also correlated with the MES regions. This finding highlights intratumoral PN/MES heterogeneity that correlates with activation of NF- κ B and macrophages/microglial involvement in GBM.

DISCUSSION

Differential Molecular Signatures in GSCs and GBMs

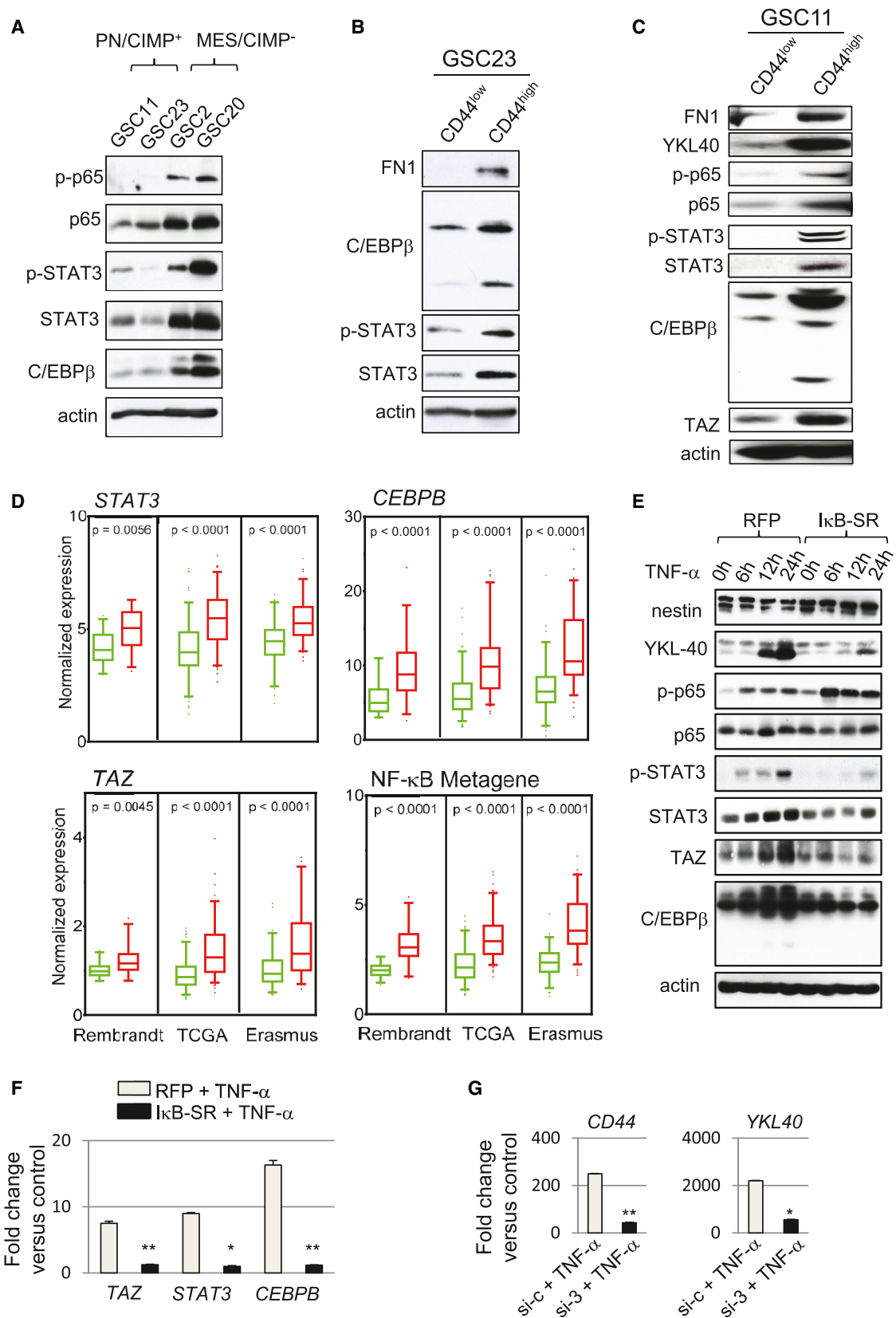
Whereas gene expression profiling of GBM has consistently shown the PN and MES subtypes, parallel efforts on GSCs have been limited, and mouse models representative of transcriptome subtypes of GBM are only beginning to emerge (Chow et al., 2011; Friedmann-Morvinski et al., 2012; Koso et al., 2012; Liu et al., 2011). In this report, we demonstrate that with the exception of a few, GSCs in general show gene expression and epigenetic profile differences from their parental tumors and that the majority of the GSCs exhibit an overall PN/CIMP⁺ signature despite originating from predominantly MES/CIMP⁻ GBMs. Placement of these PN/CIMP⁺ GSCs in intracranial xenografts did not restore the MES phenotype of the parental tumor, indicating a potential shortcoming of immunocompromised xenograft models to fully recapitulate the human tumor microenvironment (Magee et al., 2012). We could not ascertain the CIMP status of the xenografts because of technical difficulties given the small size of these tumors. Although TNF- α /NF- κ B activation induced MES differentiation, it did not alter CIMP methylation patterns, suggesting that other tumor microenvironment-derived cytokines could play a role in this process. Coupled with recent reports that resetting the epigenome of GSCs can cause remarkable changes in their malignant behavior (Stricker et al., 2013), future studies utilizing GSCs as a model system should take these factors into consideration.

MES Differentiation Is Mediated by NF- κ B Induction of Master TFs

In addition to the identification of a role for NF- κ B in inducing the MES signature, we show that this occurs via the induction of STAT3, C/EBP β , and TAZ, although it remains to be seen if the radioresistance mediated by NF- κ B is also dependent on these master TFs. Interestingly, these same TFs (with the exception of TAZ) play prominent roles in inflammatory response, and past studies have shown considerable crosstalk between these TFs. For example, NF- κ B promotes an inflammatory response through secretion of TNF- α , IL-1 β , and IL-6, of which IL-6 triggers STAT3 activation (Ben-Neriah and Karin, 2011; Hayden and Ghosh, 2012). Conversely, studies have shown that nuclear translocation of NF- κ B is dependent on acetylation of NF- κ B by

intracranial administration of TNF- α (2 ng/mouse) 72 hr prior to irradiation and once every 2 weeks thereafter. Horizontal black bar shows average radiance (photons/s/cm²/sr) with various treatments and time points. Error bar indicates \pm SEM. t test was used to assess statistical significance. **p < 0.005; NS, not significant.

See also Figure S5.



(legend on next page)

p300, which requires STAT3 activation (Gravendeel et al., 2009). The interdependency of NF- κ B and C/EBP β has also been previously reported in other studies (Acosta et al., 2008; Kuilman et al., 2008). While we show that TNF- α can be derived from macrophages/microglia, it is noteworthy that these cell types themselves exhibit plasticity and can be polarized to a proinflammatory (M1) or anti-inflammatory (M2) phenotype in the brain microenvironment (Li and Graeber, 2012; Wu et al., 2010). Because most GBMs arise de novo without prior clinical history of a lower grade tumor, it is difficult to study tumor evolution in GBM, that is, whether a MES tumor evolved from an early stage PN tumor is difficult to ascertain and the characteristics and the influence of the microenvironment in the early stages of a GBM are virtually unknown. Here we show evidence for the transcriptional plasticity of the PN and MES states by IHC analysis of tumors that had regions of both PN and MES markers and their correlation to NF- κ B activation and infiltration of macrophages/microglia. Consistent with our findings, recent studies have shown that the MES subclass of GBMs exhibit a high degree of necrosis (Cooper et al., 2012) and macrophages/microglial infiltration (Engler et al., 2012; Li et al., 2012). In addition, tumor evolutionary dynamics have been shown in a recent report wherein multiple transcriptome signatures were found within the same tumor (Sottoriva et al., 2013). We found that in some cases, MES/CIMP⁻ GSCs showed constitutive MES signatures even in instances where *NF1* mutations were not seen (e.g., GSCs 2 and 20) and when removed from the microenvironment, suggesting that cell intrinsic mechanisms that sustain the MES network also exist.

Association of the MES Signature, CD44, and NF- κ B Signaling with Radiation Resistance

Patients with GBM currently undergo standard treatment consisting of maximal surgical resection, combined radiation and chemotherapy, and adjuvant chemotherapy with temozolomide (Furnari et al., 2007; Hegi et al., 2005). Radiation has been a mainstay of GBM treatment for decades and the exact molecular mechanisms driving resistance in GBMs is unknown. Our previous studies have shown that patients with a MES signature belong to the poor prognosis subclass and are resistant to standard treatments (Colman et al., 2010) and that PN tumors can recur in a MES state (Phillips et al., 2006). Here we show that PN/CIMP⁺ GSCs under specific conditions can undergo MES differentiation, with associated radioresistance. Importantly,

we show that in newly diagnosed GBM, an increased MES metagene, CD44 expression, or NF- κ B activation is associated with poor radiation response and shorter survival even in the absence of *IDH1* mutation. Although NF- κ B has been previously implicated in GBM (Bredel et al., 2006, 2011; Park et al., 2009), our studies identify a role for NF- κ B in mediating radiation resistance. We speculate that global MES differentiation induced by NF- κ B parallels activation of checkpoint pathways, leading to enhanced DNA damage repair and unperturbed cell cycle progression in response to IR. Moreover, given that NF- κ B has been shown to mediate antiapoptotic effects and DNA damage repair (Magné et al., 2006), it is conceivable that this pathway acts as a potential link between MES differentiation and radioresistance. In the context of previous studies showing that the CD133⁺ GSCs are resistant to radiation (Bao et al., 2006), and even more efficiently under the influence of the brain microenvironment (Jamal et al., 2012), it remains to be seen whether CD133⁺ subpopulation within the CD44^{high} GSCs represents a refinement of the radioresistant cell types.

In summary (Figure 8B), we show that although GBM patient tumors appear predominantly MES/CIMP⁻ at presentation or progression, the GSCs derived from these tumors using a standard isolation procedure tend to be PN/CIMP⁺ (despite absence of the *IDH1* mutation), suggesting that tumor microenvironmental factors in humans may induce a MES/CIMP⁻ signature. We further show that in a subset of the PN/CIMP⁻ GSCs, MES differentiation with associated enrichment of CD44-expressing subpopulations and radioresistance can be induced in an NF- κ B-dependent fashion. Our data suggest that inhibition of NF- κ B activation can directly affect radioresistance and presents an attractive therapeutic target for GBM.

EXPERIMENTAL PROCEDURES

GSCs Isolation and Cell Culture

Freshly resected tumor tissues were enzymatically and mechanically dissociated into single cells and grown in DMEM/F12 media supplemented with B27 (Invitrogen), EGF (20 ng/ml), and bFGF (20 ng/ml). After 2 to 4 weeks, free-floating neurospheres were collected and thereafter routinely cultured in the above-mentioned neurosphere media, with dissociation to single cells every 5–6 days. For growth factor comparison, PDGF (R&D Systems) was used at a final concentration of 10 ng/ml. For cytokine treatment, GSCs were dissociated into single cells with Accutase (Sigma Aldrich) and treated with various concentrations and durations as indicated in figure legends. IL-6, IL-8, IL-10, and TGF- β were obtained from R&D Systems, and TNF- α was from Sigma

Figure 6. NF- κ B Controls Master TFs of MES Differentiation in GSCs

- (A) Western blot analysis of phosphorylated p65 (ser 536), total p65, phosphorylated STAT3 (Tyr 705), STAT3, and C/EBP β in GSCs is shown.
 (B and C) Western blot analysis using indicated antibodies was performed on GSC23 (B) and 11 (C) sorted for CD44^{high} or CD44^{low} subpopulations.
 (D) Box plots of normalized expression of *STAT3*, *CEBPB*, *TAZ*, and NF- κ B metagene in *CD44*^{low} (green boxes) or *CD44*^{high} (red boxes) tumors from multiple data sets as indicated are shown. Boxes show median 25th and 75th percentiles, while whiskers represent the 5th and the 95th percentiles. Outliers are shown as individual points. p value was determined using a nonparametric Wilcoxon test. For the NF- κ B metagene, the average expression of 38 NF- κ B family members and targets (see Supplemental Experimental Procedures) was condensed into a metagene and plotted. Wilcoxon signed-rank test was used to test statistical significance.
 (E) Time course western blot analysis of indicated antibodies after TNF- α treatment in GSC11 transduced with RFP or κ B-SR adenovirus 24 hr prior to TNF- α treatment is shown.
 (F) qRT-PCR analysis of MES signature master TFs *STAT3*, *CEBPB*, and *TAZ* in GSC11 treated with TNF- α with or without pretreatment with RFP or κ B-SR adenovirus is shown. Error bar indicates \pm SD. t test was used for statistical significance. *p < 0.05 and **p < 0.005.
 (G) qRT-PCR analysis of *YKL40* and *CD44* after knockdown of all three master TFs (*STAT3*, *C/EBP β* , and *TAZ*) in GSC11 is shown. Cells were treated with siRNA 72 hr prior to treatment with TNF- α for an additional 24 hr. Error bar indicates \pm SD. t test was used for statistical significance. *p < 0.05 and **p < 0.005. See also Figure S6.

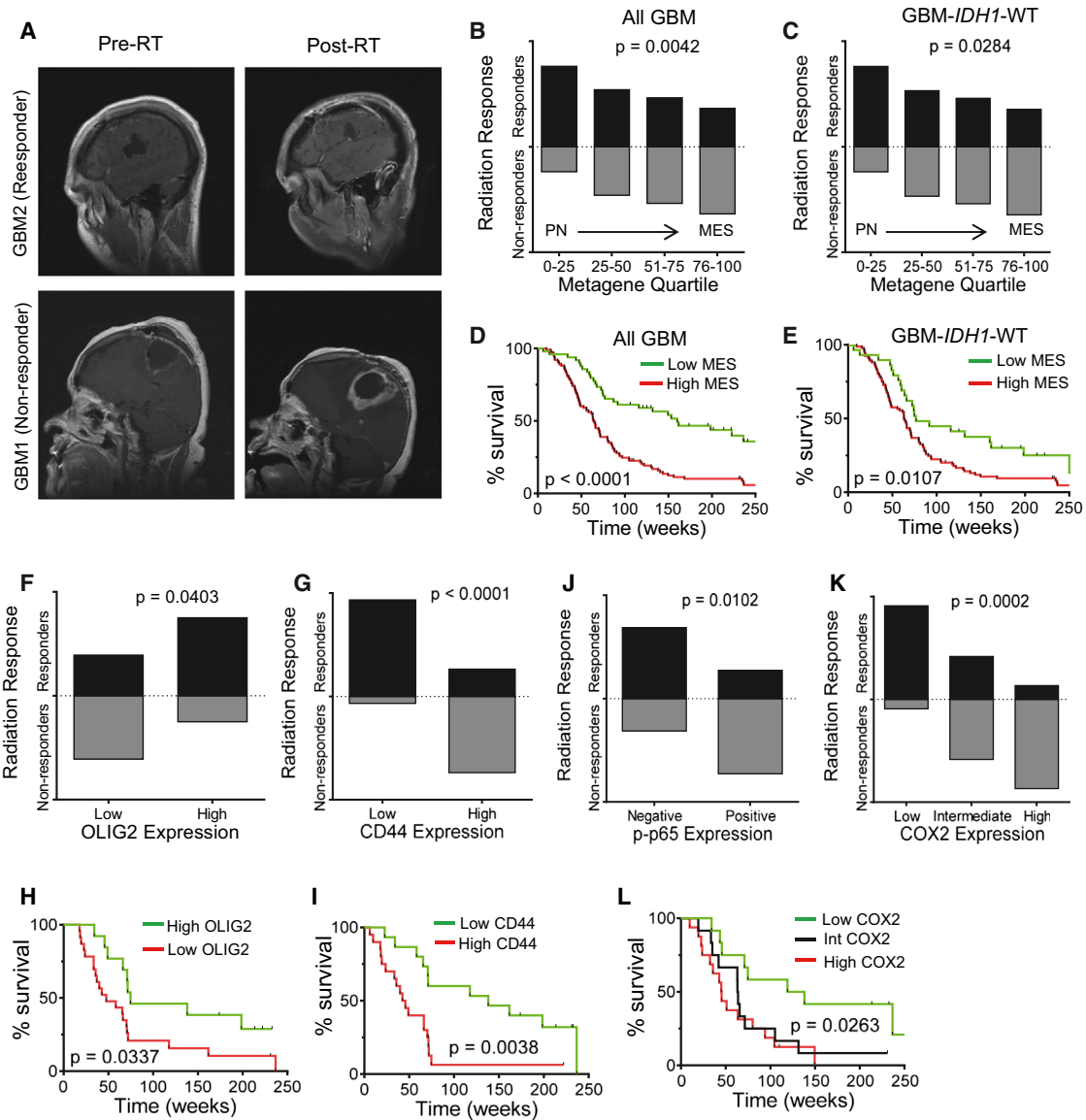


Figure 7. MES Differentiation, CD44 Levels, and NF-κB Activation Are Predictive of Radiation Response in GBM

(A) Representative MRI scans of postoperative/pre-RT and post-RT responses of patients typically classified as responders or nonresponders are shown. (B) Box plots show the proportion of patients classified as responders or non-responders against the PN/MES metagene quartiles in all newly diagnosed GBM cases (n = 149). Chi-square test was used to assess statistical significance. (C) Box plot is shown for *IDH1* WT cases (n = 121). (D) Kaplan Meier curves show survival of newly diagnosed patients based on PN/MES metagene scores. Low MES represents the bottom one-third of the cases whereas high MES was the top two-thirds. Log rank test was used to assess statistical significance. (E) Kaplan Meier curves showing survival of newly diagnosed GBM-*IDH1* WT patients based on PN/MES metagene scores. (F–L) Bar graph shows the proportion of OLIG2 (F), CD44 (G), p-p65 (J), and COX2 (K) expression in newly diagnosed GBM-*IDH1* WT patients classified as radiation responders or nonresponders. Proportions of patients who responded or did not respond were compared using chi-square test. Kaplan Meier curves show survival of newly diagnosed GBM-*IDH1* WT patients based on OLIG2 (H), CD44 (I), and COX2 (L). See also Figure S7 and Tables S6–S8.

Aldrich. RFP and κB-SR adenovirus were obtained from Vector Biolabs. The use of human tumor tissue samples and all other tumor-related studies were conducted in accordance with the protocols approved by the Institutional Review Board at the UT, M.D. Anderson Cancer Center, or the Medical Ethical Committee at the University Medical Center Groningen. The use of the tissues for the experiments involving isolation of GSCs, DNA and RNA isolation, and/or IHC on human tumors was exempt from requiring consent as per the MDACC

Institutional Review Board. Patient materials at UMCG were obtained after routine diagnostics, coded according to the National Code for the Good Use of Patient Material, and were exempt from informed consent.

Microarray and Bioinformatic Analyses

RNA labeling and hybridization to Affymetrix HGU133 version 2.0 gene-chips was performed by Expression Analysis (Durham, NC). Raw .cel files

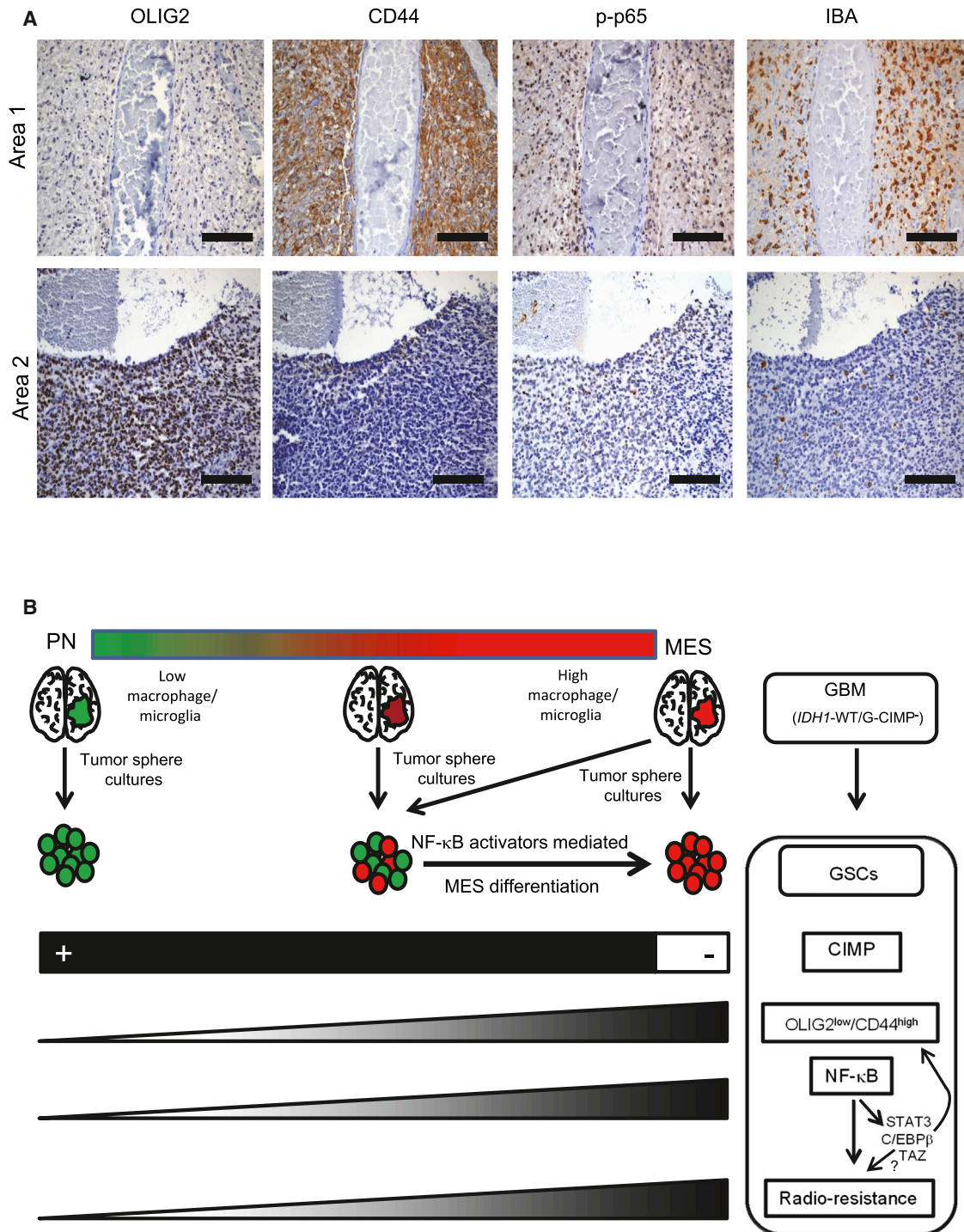


Figure 8. Features Associated with MES Differentiation Induced by NF-κB in GBM

(A) Consecutive 5 μm sections were stained for various markers by IHC. Two independent areas within a same tumor are shown for mutual exclusive expression of OLIG2 from CD44, p-p65, and IBA. Scale bar: 100 μm.

(B) Cartoon shows a summary of our findings. We propose that GSCs when isolated from the microenvironment may differ in their molecular signatures from the parental tumor. Whereas GBMs at the extreme ends of the PN/MES axis will likely contain (and enrich for) GSCs with similar signatures to the parental tumor, GBMs with intermediate to high MES signatures enrich for PN GSCs that are maintained in a MES state in the human tumor microenvironment (by cell types such as macrophages/microglia). These PN GSCs also tend to be CIMP⁺ although derived from G-CIMP⁻ tumors that lack the *IDH1* mutation. MES differentiation, CD44 enrichment, and radioresistance can be induced in PN/CIMP⁻ GSCs by activation of NF-κB and downstream master TFs (STAT3, C/EBPβ, and TAZ). In contrast, MES GSCs are CIMP⁻, predominantly express CD44, are radioresistant, and exhibit constitutive activation of NF-κB and downstream master TFs. See also Table S9.

(GSE49009) were processed using R and Bioconductor (Gentleman et al., 2004), using a custom CDF (Sandberg and Larsson, 2007), with background correction, log transformation, and quantile normalization performed using the RMA algorithm. Detailed description of all other bioinformatic analyses is described in Supplemental Experimental Procedures.

Xenograft Models and Treatments

GSCs were implanted intracranially using the guide screw system in 4- to 5-week-old NOD/SCID or Foxn1^{nu} mice. After 1 week of guide screw implantation, 5×10^5 cells or fewer (as indicated) were injected intracranially in each mouse and randomly distributed between groups. A minimum of five mice was used in each group. For in vivo bioluminescent imaging, GSCs were engineered to express luciferase by transducing with pCignal lenti-CMV-luc viral particles (SABiosciences). Kinetics of tumor growth was monitored using IVIS 200 system bioluminescent imaging and tumor volume measured using Living Image 4.1 software. IR was delivered using fractionated doses (2.5 Gy \times 4) using a ⁶⁰Co teletherapy unit and a custom gig with validated dosimetry. Mice that presented neurological symptoms (i.e., hydrocephalus, seizures, inactivity, and/or ataxia) or that were moribund were sacrificed, and brains were fixed in formalin, stained with H&E to confirm the presence of tumor, and subject to IHC. All animal procedures were reviewed and approved by the Institutional Animal Care and Use Committee at the M.D. Anderson Cancer Center.

ACCESSION NUMBERS

The Gene Expression Omnibus accession number for the microarray experiments is GSE49009.

SUPPLEMENTAL INFORMATION

Supplemental Information includes Supplemental Experimental Procedures, seven figures, and nine tables and can be found with this article online at <http://dx.doi.org/10.1016/j.ccr.2013.08.001>.

ACKNOWLEDGMENTS

We would like to acknowledge the Caroline Ross Endowment Fellowship, the American Brain Tumor Association Basic Research Fellowship, the Odyssey Special Fellowship, and the MDACC Brain Tumor SPORE Career Development grant (to K.P.L.B.); the Brain Tumor Funders' Collaborative, the Dr. Marnie Rose Foundation, and the National Brain Tumor Society (to K.A.); the V Foundation and SPORE grant P50CA127001 from NIH/NCI (to K.A. and H.C.); the Huntsman Cancer Foundation (to H.C.); the Ben and Cathy Ivy Foundation Research Award (to F.F.L., K.A., and E.P.S.); the SPORE Animal Core grant (to F.F.L.); grant R01-CA1208113 from NIH/NCI (to A.H.); and Dutch Cancer Society grant RUG 2011-5150 (to V.B., H.W.B., and W.F.D.) for their generous support. We thank Alicia Ledoux, Bhavna Singh, and Susan Cweren for histology; Verlene Henry for animal injections; and the Flow Cytometry & Cellular Imaging Core Facility, Small Animal Imaging Facility, and the Division of Surgery Pathology Core Facility (all at MDACC supported by P30-CA016672) for technical support. We apologize for not citing some original references because of space limitations. H.S.P. is an employee and stockholder of Roche/Genentech.

Received: May 11, 2012

Revised: June 24, 2013

Accepted: August 1, 2013

Published: August 29, 2013

REFERENCES

Acosta, J.C., O'Loughlin, A., Banito, A., Gujjarro, M.V., Augert, A., Raguz, S., Fumagalli, M., Da Costa, M., Brown, C., Popov, N., et al. (2008). Chemokine signaling via the CXCR2 receptor reinforces senescence. *Cell* 133, 1006–1018.

Bao, S., Wu, Q., McLendon, R.E., Hao, Y., Shi, Q., Hjelmeland, A.B., Dewhirst, M.W., Bigner, D.D., and Rich, J.N. (2006). Glioma stem cells promote radioresistance by preferential activation of the DNA damage response. *Nature* 444, 756–760.

Ben-Neriah, Y., and Karin, M. (2011). Inflammation meets cancer, with NF- κ B as the matchmaker. *Nat. Immunol.* 12, 715–723.

Bhat, K.P., Salazar, K.L., Balasubramanian, V., Wani, K., Heathcock, L., Hollingsworth, F., James, J.D., Gumin, J., Diefes, K.L., Kim, S.H., et al. (2011). The transcriptional coactivator TAZ regulates mesenchymal differentiation in malignant glioma. *Genes Dev.* 25, 2594–2609.

Bredel, M., Bredel, C., Juric, D., Duran, G.E., Yu, R.X., Harsh, G.R., Vogel, H., Recht, L.D., Scheck, A.C., and Sikic, B.I. (2006). Tumor necrosis factor- α -induced protein 3 as a putative regulator of nuclear factor- κ B-mediated resistance to O₆-alkylating agents in human glioblastomas. *J. Clin. Oncol.* 24, 274–287.

Bredel, M., Scholtens, D.M., Yadav, A.K., Alvarez, A.A., Renfrow, J.J., Chandler, J.P., Yu, I.L., Carro, M.S., Dai, F., Tagge, M.J., et al. (2011). NFKBIA deletion in glioblastomas. *N. Engl. J. Med.* 364, 627–637.

Brescia, P., Richichi, C., and Pelicci, G. (2012). Current strategies for identification of glioma stem cells: adequate or unsatisfactory? *J. Oncol.* 2012, 376894.

Carro, M.S., Lim, W.K., Alvarez, M.J., Bollo, R.J., Zhao, X., Snyder, E.Y., Sulman, E.P., Anne, S.L., Doetsch, F., Colman, H., et al. (2010). The transcriptional network for mesenchymal transformation of brain tumours. *Nature* 463, 318–325.

Charles, N.A., Holland, E.C., Gilbertson, R., Glass, R., and Kettenmann, H. (2011). The brain tumor microenvironment. *Glia* 59, 1169–1180.

Chen, J., McKay, R.M., and Parada, L.F. (2012). Malignant glioma: lessons from genomics, mouse models, and stem cells. *Cell* 149, 36–47.

Chow, L.M., Endersby, R., Zhu, X., Rankin, S., Qu, C., Zhang, J., Broniscer, A., Ellison, D.W., and Baker, S.J. (2011). Cooperativity within and among Pten, p53, and Rb pathways induces high-grade astrocytoma in adult brain. *Cancer Cell* 19, 305–316.

Colman, H., Zhang, L., Sulman, E.P., McDonald, J.M., Shooshtari, N.L., Rivera, A., Popoff, S., Nutt, C.L., Louis, D.N., Cairncross, J.G., et al. (2010). A multi-gene predictor of outcome in glioblastoma. *Neuro-oncol.* 12, 49–57.

Cooper, L.A., Gutman, D.A., Long, Q., Johnson, B.A., Cholleti, S.R., Kurc, T., Saltz, J.H., Brat, D.J., and Moreno, C.S. (2010). The proneural molecular signature is enriched in oligodendrogliomas and predicts improved survival among diffuse gliomas. *PLoS ONE* 5, e12548.

Cooper, L.A., Gutman, D.A., Chisolm, C., Appin, C., Kong, J., Rong, Y., Kurc, T., Van Meir, E.G., Saltz, J.H., Moreno, C.S., and Brat, D.J. (2012). The tumor microenvironment strongly impacts master transcriptional regulators and gene expression class of glioblastoma. *Am. J. Pathol.* 180, 2108–2119.

Daginakatte, G.C., and Gutmann, D.H. (2007). Neurofibromatosis-1 (Nf1) heterozygous brain microglia elaborate paracrine factors that promote Nf1-deficient astrocyte and glioma growth. *Hum. Mol. Genet.* 16, 1098–1112.

Dennis, G., Jr., Sherman, B.T., Hosack, D.A., Yang, J., Gao, W., Lane, H.C., and Lempicki, R.A. (2003). DAVID: Database for Annotation, Visualization, and Integrated Discovery. *Genome Biol.* 4, 3.

Engler, J.R., Robinson, A.E., Smirnov, I., Hodgson, J.G., Berger, M.S., Gupta, N., James, C.D., Molinaro, A., and Phillips, J.J. (2012). Increased microglia/macrophage gene expression in a subset of adult and pediatric astrocytomas. *PLoS ONE* 7, e43339.

Friedmann-Morvinski, D., Bushong, E.A., Ke, E., Soda, Y., Marumoto, T., Singer, O., Ellisman, M.H., and Verma, I.M. (2012). Dedifferentiation of neurons and astrocytes by oncogenes can induce gliomas in mice. *Science* 338, 1080–1084.

Furnari, F.B., Fenton, T., Bachoo, R.M., Mukasa, A., Stommel, J.M., Stegh, A., Hahn, W.C., Ligon, K.L., Louis, D.N., Brennan, C., et al. (2007). Malignant astrocytic glioma: genetics, biology, and paths to treatment. *Genes Dev.* 21, 2683–2710.

Gentleman, R.C., Carey, V.J., Bates, D.M., Bolstad, B., Dettling, M., Dudoit, S., Ellis, B., Gautier, L., Ge, Y., Gentry, J., et al. (2004). Bioconductor: open software development for computational biology and bioinformatics. *Genome Biol.* 5, R80.

- Gravendeel, L.A., Kouwenhoven, M.C., Gevaert, O., de Rooij, J.J., Stubbs, A.P., Duijm, J.E., Daemen, A., Bleeker, F.E., Bralten, L.B., Kloosterhof, N.K., et al. (2009). Intrinsic gene expression profiles of gliomas are a better predictor of survival than histology. *Cancer Res.* 69, 9065–9072.
- Hayden, M.S., and Ghosh, S. (2012). NF- κ B, the first quarter-century: remarkable progress and outstanding questions. *Genes Dev.* 26, 203–234.
- Hegi, M.E., Diserens, A.C., Gorlia, T., Hamou, M.F., de Tribolet, N., Weller, M., Kros, J.M., Hainfellner, J.A., Mason, W., Mariani, L., et al. (2005). MGMT gene silencing and benefit from temozolomide in glioblastoma. *N. Engl. J. Med.* 352, 997–1003.
- Hjelmeland, A.B., Wu, Q., Wickman, S., Eyler, C., Heddleston, J., Shi, Q., Lathia, J.D., Macsworlds, J., Lee, J., McLendon, R.E., and Rich, J.N. (2010). Targeting A20 decreases glioma stem cell survival and tumor growth. *PLoS Biol.* 8, e1000319.
- Huse, J.T., Phillips, H.S., and Brennan, C.W. (2011). Molecular subclassification of diffuse gliomas: seeing order in the chaos. *Glia* 59, 1190–1199.
- Jamal, M., Rath, B.H., Tsang, P.S., Camphausen, K., and Tofilon, P.J. (2012). The brain microenvironment preferentially enhances the radioresistance of CD133(+) glioblastoma stem-like cells. *Neoplasia* 14, 150–158.
- Jijiwa, M., Demir, H., Gupta, S., Leung, C., Joshi, K., Orozco, N., Huang, T., Yildiz, V.O., Shibahara, I., de Jesus, J.A., et al. (2011). CD44v6 regulates growth of brain tumor stem cells partially through the AKT-mediated pathway. *PLoS ONE* 6, e24217.
- Koso, H., Takeda, H., Yew, C.C., Ward, J.M., Nariai, N., Ueno, K., Nagasaki, M., Watanabe, S., Rust, A.G., Adams, D.J., et al. (2012). Transposon mutagenesis identifies genes that transform neural stem cells into glioma-initiating cells. *Proc. Natl. Acad. Sci. USA* 109, E2998–E3007.
- Kuilman, T., Michaloglou, C., Vredeveld, L.C., Douma, S., van Doorn, R., Desmet, C.J., Aarden, L.A., Mooi, W.J., and Peeper, D.S. (2008). Oncogene-induced senescence relayed by an interleukin-dependent inflammatory network. *Cell* 133, 1019–1031.
- Li, W., and Graeber, M.B. (2012). The molecular profile of microglia under the influence of glioma. *Neuro-oncol.* 14, 958–978.
- Li, B., Senbabaoglu, Y., Peng, W., Yang, M.L., Xu, J., and Li, J.Z. (2012). Genomic estimates of aneuploid content in glioblastoma multiforme and improved classification. *Clin. Cancer Res.* 18, 5595–5605.
- Liu, C., Sage, J.C., Miller, M.R., Verhaak, R.G., Hippenmeyer, S., Vogel, H., Foreman, O., Bronson, R.T., Nishiyama, A., Luo, L., and Zong, H. (2011). Mosaic analysis with double markers reveals tumor cell of origin in glioma. *Cell* 146, 209–221.
- Lu, C., Ward, P.S., Kapoor, G.S., Rohle, D., Turcan, S., Abdel-Wahab, O., Edwards, C.R., Khanin, R., Figueroa, M.E., Melnick, A., et al. (2012). IDH mutation impairs histone demethylation and results in a block to cell differentiation. *Nature* 483, 474–478.
- Magee, J.A., Piskounova, E., and Morrison, S.J. (2012). Cancer stem cells: impact, heterogeneity, and uncertainty. *Cancer Cell* 21, 283–296.
- Magné, N., Toillon, R.A., Bottero, V., Didelot, C., Houtte, P.V., Gérard, J.P., and Peyron, J.F. (2006). NF- κ B modulation and ionizing radiation: mechanisms and future directions for cancer treatment. *Cancer Lett.* 231, 158–168.
- Markovic, D.S., Vinnakota, K., van Rooijen, N., Kiwit, J., Synowitz, M., Glass, R., and Kettenmann, H. (2011). Minocycline reduces glioma expansion and invasion by attenuating microglial MT1-MMP expression. *Brain Behav. Immun.* 25, 624–628.
- Mir, S.E., De Witt Hamer, P.C., Krawczyk, P.M., Balaj, L., Claes, A., Niers, J.M., Van Tilborg, A.A., Zwinderman, A.H., Geerts, D., Kaspers, G.J., et al. (2010). In silico analysis of kinase expression identifies WEE1 as a gatekeeper against mitotic catastrophe in glioblastoma. *Cancer Cell* 18, 244–257.
- Murat, A., Migliavacca, E., Hussain, S.F., Heimberger, A.B., Desbaillets, I., Hamou, M.F., Rüegg, C., Stupp, R., Delorenzi, M., and Hegi, M.E. (2009). Modulation of angiogenic and inflammatory response in glioblastoma by hypoxia. *PLoS ONE* 4, e5947.
- Noushmehr, H., Weisenberger, D.J., Diefes, K., Phillips, H.S., Pujara, K., Berman, B.P., Pan, F., Pelloski, C.E., Sulman, E.P., Bhat, K.P., et al.; Cancer Genome Atlas Research Network. (2010). Identification of a CpG island methylator phenotype that defines a distinct subgroup of glioma. *Cancer Cell* 17, 510–522.
- Park, S., Hatanpaa, K.J., Xie, Y., Mickey, B.E., Madden, C.J., Raisanen, J.M., Ramnarain, D.B., Xiao, G., Saha, D., Boothman, D.A., et al. (2009). The receptor interacting protein 1 inhibits p53 induction through NF- κ B activation and confers a worse prognosis in glioblastoma. *Cancer Res.* 69, 2809–2816.
- Pelloski, C.E., Mahajan, A., Maor, M., Chang, E.L., Woo, S., Gilbert, M., Colman, H., Yang, H., Ledoux, A., Blair, H., et al. (2005). YKL-40 expression is associated with poorer response to radiation and shorter overall survival in glioblastoma. *Clin. Cancer Res.* 11, 3326–3334.
- Phillips, H.S., Kharbanda, S., Chen, R., Forrest, W.F., Soriano, R.H., Wu, T.D., Misra, A., Nigro, J.M., Colman, H., Soroceanu, L., et al. (2006). Molecular subclasses of high-grade glioma predict prognosis, delineate a pattern of disease progression, and resemble stages in neurogenesis. *Cancer Cell* 9, 157–173.
- Pietsch, T., and Wiestler, O.D. (1997). Molecular neuropathology of astrocytic brain tumors. *J. Neurooncol.* 35, 211–222.
- Riddick, G., and Fine, H.A. (2011). Integration and analysis of genome-scale data from gliomas. *Nat Rev Neurol* 7, 439–450.
- Sandberg, R., and Larsson, O. (2007). Improved precision and accuracy for microarrays using updated probe set definitions. *BMC Bioinformatics* 8, 48.
- Son, M.J., Woolard, K., Nam, D.H., Lee, J., and Fine, H.A. (2009). SSEA-1 is an enrichment marker for tumor-initiating cells in human glioblastoma. *Cell Stem Cell* 4, 440–452.
- Sottoriva, A., Spiteri, I., Piccirillo, S.G., Touloumis, A., Collins, V.P., Marioni, J.C., Curtis, C., Watts, C., and Tavaré, S. (2013). Intratumor heterogeneity in human glioblastoma reflects cancer evolutionary dynamics. *Proc. Natl. Acad. Sci. USA* 110, 4009–4014.
- Stopschinski, B.E., Beier, C.P., and Beier, D. (2012). Glioblastoma cancer stem cells - From concept to clinical application. *Cancer Lett.* Published online June 2, 2012. <http://dx.doi.org/10.1016/j.canlet.2012.05.033>.
- Stricker, S.H., Feber, A., Engström, P.G., Carén, H., Kurian, K.M., Takahama, Y., Watts, C., Way, M., Dirks, P., Bertone, P., et al. (2013). Widespread resetting of DNA methylation in glioblastoma-initiating cells suppresses malignant cellular behavior in a lineage-dependent manner. *Genes Dev.* 27, 654–669.
- Subramanian, A., Tamayo, P., Mootha, V.K., Mukherjee, S., Ebert, B.L., Gillette, M.A., Paulovich, A., Pomeroy, S.L., Golub, T.R., Lander, E.S., and Mesirov, J.P. (2005). Gene set enrichment analysis: a knowledge-based approach for interpreting genome-wide expression profiles. *Proc. Natl. Acad. Sci. USA* 102, 15545–15550.
- Turcan, S., Rohle, D., Goenka, A., Walsh, L.A., Fang, F., Yilmaz, E., Campos, C., Fabius, A.W., Lu, C., Ward, P.S., et al. (2012). IDH1 mutation is sufficient to establish the glioma hypermethylator phenotype. *Nature* 483, 479–483.
- Verhaak, R.G., Hoadley, K.A., Purdom, E., Wang, V., Qi, Y., Wilkerson, M.D., Miller, C.R., Ding, L., Golub, T., Mesirov, J.P., et al.; Cancer Genome Atlas Research Network. (2010). Integrated genomic analysis identifies clinically relevant subtypes of glioblastoma characterized by abnormalities in PDGFRA, IDH1, EGFR, and NF1. *Cancer Cell* 17, 98–110.
- Wu, A., Wei, J., Kong, L.Y., Wang, Y., Priebe, W., Qiao, W., Sawaya, R., and Heimberger, A.B. (2010). Glioma cancer stem cells induce immunosuppressive macrophages/microglia. *Neuro-oncol.* 12, 1113–1125.
- Zöller, M. (2011). CD44: can a cancer-initiating cell profit from an abundantly expressed molecule? *Nat. Rev. Cancer* 11, 254–267.